Wigner Spectrograms for Femtosecond Pulse-Shaped Heterodyne and Autocorrelation Measurements

Shaul Mukamel, Calin Ciordas-Ciurdariu, and Vadim Khidekel

Abstract—**We develop a mixed time-frequency representation for the calculation and interpretation of coherent optical measurements. Heterodyne and autocorrelation signals are expressed in terms of a mixed material response function and a Wigner distribution for the incoming pulses, the detected field, and the gating device. Applications to pump-probe spectroscopy, spontaneous light emission, and impulsive four-wave mixing (three-pulse echoes) are discussed.**

I. Introduction

RAPID progress in pulse-shaping techniques has made it possible to control the temporal profiles as well as the phases of optical fields with a remarkable accuracy [1]–[6]. Optical spectroscopy explores the coupling of an external electromagnetic field $E(\boldsymbol{r},t)$ to the polarization $P(\boldsymbol{r},t)$ created in the material system. Ideal impulsive measurements in which the incoming fields are much shorter than all relevant molecular times may be directly interpreted using time-domain nonlinear response functions. In the opposite limit of stationary fields, a purely frequency-domain description in terms of optical susceptibilities is called for [7]. Formally, either representation may be extended to incorporate pulse sequences of arbitrary shape and phase by using a proper (either temporal or spectral) convolution over field envelopes. However, it is often desirable to adopt a mixed time-frequency representation in which both characteristics of the field and the response function are highlighted. In the snapshot limit of pump-probe spectroscopy, for example, the field is short compared with nuclear motions and has a narrow bandwidth compared with the optical lineshape. It is essential to consider both spectral and temporal profiles of the field in order to realize this important limiting case [7].

In this paper, we show how a mixed time-frequency representation for the material response function, as well as for the incoming fields, the signal field, and the gating device, may be effectively used in the calculation of various optical signals. This representation clarifies the role of field frequency and temporal profiles on the induced polarization and provides valuable information about the signal (e.g., its time-dependent spectrum). The present representation is particularly suitable for the description of coherent optical control of dynamical events.[1]

We shall expand the electric field and the polarization in the form

$$E(\boldsymbol{r},t)=\sum_j \mathcal{E}_j(t)e^{i\boldsymbol{k}_j\boldsymbol{r}}+\text{c.c.}$$

$$P(\boldsymbol{r},t)=\sum_j \mathcal{P}_j(t)e^{i\boldsymbol{k}_j\boldsymbol{r}}+\text{c.c.}$$

where $\mathcal{E}_j(t)$ and $\mathcal{P}_j(t)$ are the complex-valued *analytic* field and polarization, respectively [8]. The field envelope $\mathcal{E}_j(t)$ can be further represented in the form $\mathcal{E}_j(t)=\tilde{\mathcal{E}}_j(t)e^{-i\omega_j t}$, where $\tilde{\mathcal{E}}_j(t)$ is a slow-varying envelope and ω_j is the carrier frequency.

In the simplest detection scheme of optical signals, one measures the time-integrated intensity of the field generated by the sample in a given direction $\boldsymbol{k}_j$:

$$I(\boldsymbol{k}_j)\propto\int\langle\mathcal{E}_j^*(t)\mathcal{E}_j(t)\rangle\,dt. \tag{1}$$

Time-integrated detection is commonly used in wave-mixing experiments, such as photon echoes [9]. However, time-integrated photon echo signals do not contain sufficient information to establish the correct form of the spectral density responsible for optical dephasing [10]. Additional, most valuable microscopic information may be obtained by time-gated (or time-resolved) detection [11], achieved by overlapping the total response with a narrow gate pulse, which provides the temporal profile of the signal.

Mixed time-frequency pictures can be obtained if between a sample and a detector one puts a spectral and/or temporal filter centered near some controlled frequency and time [12]. Several approaches to measure both time and frequency properties of nonlinear response in semiconductors are discussed in [13]. These measurements are based on overlapping the signal emitted by the sample with a known reference pulse, which plays the role of a temporal gate.

Mixed time-frequency measurements were first introduced in acoustics, in analysis of sound and speech [14]. They were later extended to other fields. Various theoretical methods for describing joint temporal and spectral properties of signals have been developed. The chronocyclic representation [15], [16], known also as the Wigner distribution [17]–[20], was applied to optical measurements, and it was shown that signals

Manuscript received February 1, 1996; revised April 4, 1996. The work was supported by the National Science Foundation and the Air Force Office of Scientific Research.

S. Mukamel and V. Khidekel are with the Department of Chemistry, University of Rochester, Rochester, NY 14627 USA.

C. Ciordas-Ciurdariu is with the Department of Physics, University of Rochester, Rochester, NY 14627 USA.

Publisher Item Identifier S 0018-9197(96)05583-2.

[1]It is possible also to adopt a Wigner representation of wavepackets in coordinate-momentum (rather than time-frequency) space. This provides a very useful description but will not be discussed here (see [7])

can be conveniently expressed in terms of this function. The Wigner distribution of the field is defined as

$$\mathcal{W}_j(t,\omega) \equiv \int_{-\infty}^{\infty} \mathcal{E}_j^*(t-\tau/2)\mathcal{E}_j(t+\tau/2)e^{i\omega\tau}\,d\tau.$$

This function directly shows what fraction of the field energy is contained in a given time and frequency window and provides natural means for the microscopic description and analysis of optical signals. Integrating the Wigner distribution over frequencies gives the instantaneous field energy

$$\int_{-\infty}^{\infty} \mathcal{W}_j(t,\omega)\,d\omega = 2\pi|\mathcal{E}_j(t)|^2$$

while integrating it over time gives the energy density spectrum

$$\int_{-\infty}^{\infty} \mathcal{W}_j(t,\omega)\,dt = |\mathcal{E}_j(\omega)|^2, \quad \mathcal{E}_j(\omega) \equiv \int_{-\infty}^{\infty} \mathcal{E}_j(t)e^{i\omega t}\,dt.$$

The relevant information contained in a pulse goes beyond these two integrated quantities. For example, it was shown [6] that two chirped fields with nearly identical temporal and spectral profiles yield different pump-probe signals for molecular iodine in the gas phase.

The properties of the Wigner distribution have been known for a long time. It was, however, argued that its practical use may be limited, since it requires the knowledge of the electric field for all times, past and future [21]. Nevertheless, the interest in using this distribution in the description of optical fields was resuscitated in the last few years, when it became apparent that it is not only a theoretical construct, but it can be actually retrieved from nonlinear experiments [15], providing, therefore, a method for characterizing a signal completely, both in time and frequency domain.

One of the first applications in which the Wigner distribution was directly measured was the detection of radar signals, where the temporal characteristics of the signal relate to the distance to the detected object, and the frequency showed its velocity. In this case, the modulus square of the Wigner function $|\mathcal{W}(t,\omega)|^2$ was measured [22], [23].

A similar technique, frequency-resolved optical gating (FROG), has been introduced [24], [25]. This method enables one to measure the FROG spectrogram

$$I_{\mathrm{FROG}}(t,\omega) \propto \left|\int_{-\infty}^{\infty} E(\tau)|E(\tau-t)|^2 \exp(-i\omega\tau)\,d\tau\right|^2. \tag{2}$$

This spectrogram can then be inverted, and the intensity and phase (or, equivalent to the phase, the instantaneous frequency) of a pulse is obtained. However, the correspondence between FROG signals and the temporal and spectral profiles of the field is not always unique [6], [24]. We shall denote any quantity that displays the joint spectral temporal profile of the field as a spectrogram.

In Section II, we consider heterodyne detection and the absorption of a weak probe pulse. We introduce the mixed time- and frequency-domain response function, which depends on both the material system and the exciting fields, and express the signal as a convolution of this response function and the Wigner representation of the probe field. Ideal time- or frequency-resolved measurements are shown to be two limiting cases of the signal in the Wigner picture. In Section III, we consider pump-probe experiments and express the signal as a convolution of the material response function and the Wigner representations of the pump and probe fields.

In Section IV, we study gated homodyne measurements and show that the signal can be expressed as a convolution of a single-gate Wigner function, which represents both the time and the spectral gates, and the Wigner distribution of the polarization. We study a general case where the field $\mathcal{E}_j(t)$ passes through both the time and the spectral gate. The incoherent autocorrelation signal, to second order in the external field, representing spontaneous light emission, is calculated. In Section V, we consider coherent autocorrelation signals and apply our formulas to the three-pulse photon echo technique. We illustrate how the signal changes upon passing through the gates and how its time or frequency characteristics can be probed by selecting the gate parameters.

II. Heterodyne Detection; Absorption of a Weak Probe

Heterodyne detection involves mixing the scattered field $\mathcal{E}_s(t)$ generated, e.g., in a multiwave-mixing process, with an additional heterodyne field $\mathcal{E}_{\mathrm{het}}(t)$. Within the slowly varying amplitude approximation, the measured field is proportional to the polarization $\mathcal{P}_s(t)$ induced in the sample by external electric fields [27]

$$\mathcal{E}_s(t) = 2\frac{\delta_{nm}\omega_s^2 - c^2 k_s^n k_s^m}{\omega_s^2 - c^2|\boldsymbol{k}_s|^2}\mathcal{P}_s(t)$$

where k_s^n and k_s^m are the nth and mth components of the wave vector $\boldsymbol{k}_s$. The signal in the $\boldsymbol{k}_s$ direction can then be written in terms of the polarization $\mathcal{P}_s(t)$ as

$$I_{\mathrm{het}} = \int_{-\infty}^{\infty} \mathcal{E}_{\mathrm{het}}^*(t)\mathcal{P}_s(t)\,dt + \mathrm{c.c.} \tag{3}$$

where

$$\mathcal{P}_s(t) = \mathrm{Tr}\{\hat{V}_s(t)\rho(-\infty)\}.$$

We have defined the dipole operator

$$\hat{V} = \sum_j \hat{V}_j \exp(i\boldsymbol{k}_j\cdot\boldsymbol{r}_j) + \mathrm{c.c.}$$

$\hat{V}(t)$ is the polarization in the Heisenberg picture, calculated with respect to the Hamiltonian with all fields present, and $\rho(-\infty)$ is the equilibrium density matrix

$$\hat{V}(t) = \exp\left\{\frac{i}{\hbar}\int_{-\infty}^{t} H(\tau)\,d\tau\right\} \cdot V(-\infty)\exp\left\{-\frac{i}{\hbar}\int_{-\infty}^{t} H(\tau)\,d\tau\right\}. \tag{4}$$

$\hat{V}_s$ is defined as the $\boldsymbol{k}_s$ component of $\hat{V}(t)$ taken *after the evolution*. Usually, the heterodyne field is a replica of one

of the incoming fields (hereafter, denoted the probe), and we expand the polarization to linear order in the probe field $\mathcal{E}_2(\tau)$

$$\mathcal{P}_s(t) = \int_{-\infty}^{\infty} d\tau\ \tilde{S}^{(1)}(t,\tau)\mathcal{E}_2(\tau) \tag{5}$$

where $\tilde{S}^{(1)}(t,\tau)$ is the response function linear in the probe [7]

$$\tilde{S}^{(1)}(t,\tau) = \frac{i}{\hbar}\theta(t-\tau)\langle[\tilde{V}_s(t), \tilde{V}_2(\tau)]\rangle.$$

$\tilde{V}_j(t)$ is the dipole operator in the interaction picture, whose evolution is given by (4), except that the Hamiltonian now excludes the probe, but includes all other fields. $\theta(t-\tau)$ is the Heaviside step function (1 for $\tau < t$, 0 for $\tau > t$). $\tilde{V}_s$ or $\tilde{V}_2$ correspond to the wavevector of the signal and the probe field, respectively. Setting $\mathcal{E}_{\text{het}} = \mathcal{E}_2$, we can write the signal (3) as

$$I_{\text{het}} = \frac{i}{\hbar}\int_{-\infty}^{\infty} dt \int_{-\infty}^{t} d\tau\ \mathcal{E}_2^*(t)\mathcal{E}_2(\tau)\langle[\tilde{V}_s(t), \tilde{V}_2(\tau)]\rangle. \tag{6}$$

This is the general expression for the heterodyne signal in a system excited by an arbitrary set of fields and a weak probe, whose envelope is identical to the heterodyne field.

We shall now recast this result using the Wigner representation. The Wigner function of the probe pulse $\mathcal{W}_2(t,\omega)$ satisfies

$$\mathcal{E}_2^*(t)\mathcal{E}_2(\tau) = \frac{1}{2\pi}\int_{-\infty}^{\infty} \mathcal{W}_2\left(\frac{t+\tau}{2}, \omega''\right)e^{i\omega''(t-\tau)}\, d\omega'' \tag{7}$$

and the heterodyne signal (6) becomes

$$I_{\text{het}} = \iint_{-\infty}^{\infty} dt\ d\tau \int_{-\infty}^{\infty} \frac{d\omega''}{2\pi}\mathcal{W}_2\left(\frac{t+\tau}{2}, \omega''\right)e^{i\omega''(t-\tau)}\tilde{S}^{(1)}(t,\tau).$$

Changing variables as $t+\tau \to 2t'', t-\tau \to \tau''$, and defining a mixed time-frequency response function

$$\tilde{S}^{(1)}(t'',\omega'') = \int_{-\infty}^{\infty} d\tau''\ \tilde{S}^{(1)}(t''+\tau''/2, t''-\tau''/2)e^{i\tau''\omega''} \tag{8}$$

we finally have

$$I_{\text{het}} = \int_{-\infty}^{\infty} dt'' \int_{-\infty}^{\infty} \frac{d\omega''}{2\pi}\mathcal{W}_2(t'',\omega'')\tilde{S}^{(1)}(t'',\omega''). \tag{9}$$

Equation (9) is our general expression for heterodyne signals, in which both the material and the field are given by a mixed time-frequency representation.

We shall now consider two limiting cases. For an impulsive probe, whose Wigner distribution is narrowly peaked at time t_0

$$\mathcal{W}_2(t',\omega') = \mathcal{W}_2\delta(t'-t_0)$$

(9) together with (8) give

$$I_{\text{het}}(t_0) = \tilde{S}^{(1)}(t_0,t_0).$$

It can be easily shown that this coincides with the conventional definition of the time-resolved signal [7]

$$I_{\text{het}}(t_0) \propto \text{Im}[\mathcal{E}_s^*(t_0)\mathcal{P}_s(t_0)]$$

provided we expand the polarization $\mathcal{P}_s(t_0)$ using (5) and assume an impulsive probe.

In the other extreme of ideal frequency-domain measurements, we assume that the probe is narrowly peaked around frequency ω_0

$$\mathcal{W}_2(t',\omega') = \mathcal{W}_2\delta(\omega'-\omega_0).$$

Equation (9) then becomes

$$I_{\text{het}}(\omega_0) = \tilde{S}^{(1)}(\omega_0,\omega_0) \tag{10}$$

where

$$\tilde{S}^{(1)}(\omega_1,\omega_2) \equiv \iint_{-\infty}^{\infty} dt_1\ dt_2\ \tilde{S}^{(1)}(t_1,t_2)e^{it_1\omega_1}e^{it_2\omega_2}.$$

Equation (10) coincides with the conventional definition of the frequency-resolved signal [7]

$$I_{\text{het}}(\omega_0) \propto \text{Im}[\mathcal{E}_s^*(\omega_0)\mathcal{P}_s(\omega_2)].$$

To show this, we expand $\mathcal{P}_s(t)$ linearly in the probe field in the frequency domain, perform the Fourier transform in t, and assume that the probe field is monochromatic.

III. Pump-Probe Spectroscopy

The heterodyne signal depends on various frequency and time parameters characterizing the incoming fields. The response function $\tilde{S}^{(1)}(t'',\omega'')$ can be expanded perturbatively in powers of the excitation fields to any desired order. $(n+2)$-wave mixing processes are described by expanding it to nth order. Pump-probe spectroscopy is a particular case of heterodyne detection, where the wavevector of the signal $\boldsymbol{k}_s$ coincides with that of the probe $\boldsymbol{k}_2$, and we have

$$\tilde{S}^{(1)}(t,\tau) = \frac{i}{\hbar}\theta(t-\tau)\langle[\tilde{V}_2(t), \tilde{V}_2(\tau)]\rangle.$$

Hereafter, we consider pump-probe spectroscopy using a weak pump, which is a special case of heterodyne-detected four-wave mixing ($n = 2$), and expand $\tilde{S}^{(1)}(t'',\omega'')$ to second order in the light field $\mathcal{E}_1^*(t)$

$$\tilde{S}^{(1)}(t'',\omega'') = \iint_{-\infty}^{\infty} d\tau'\ d\tau''S^{(3)}(t'',\omega'',\tau',\tau'')\mathcal{E}_1^*(\tau')\mathcal{E}_1(\tau'')$$

where $S^{(3)}(t'',\omega'',\tau',\tau'')$ is the third-order response function. By definition, this function vanishes for $\tau', \tau'' > t$. Note that unlike the conventional response function [7], in which all time arguments are fully ordered, only partial time ordering is retained in the function $S^{(3)}(t'',\omega'',\tau',\tau'')$; there is no specific order between the time at which the probe field interacts with the system and the times of the two interaction with the pump. Introducing in analogy to (7) the Wigner representation of the pump field $W_1(t,\omega')$, we get for the pump-probe signal

$$I_{\text{PP}} = \frac{1}{(2\pi)^2}\iiint_{-\infty}^{\infty} dt''\ d\tau'\ d\tau'' \iint_{-\infty}^{\infty} d\omega'\ d\omega''\ e^{i\omega'(\tau'-\tau'')} \cdot \mathcal{W}_1\left(\frac{\tau'+\tau''}{2}, \omega'\right)S^{(3)}(t'',\omega'',\tau',\tau'')\mathcal{W}_2(t'',\omega'').$$

Changing the variables $\tau'+\tau'' \to 2t', \tau'-\tau'' \to \tau'$, we obtain

$$I_{\mathrm{PP}} = \frac{1}{(2\pi)^2}\iiint_{-\infty}^{\infty} dt'\, dt''\, d\tau' \iint_{-\infty}^{\infty} d\omega'\, d\omega''\, e^{i\tau'\omega'} \cdot \mathcal{W}_1(t',\omega') \cdot S^{(3)}\left(t'',\omega'',t'+\frac{\tau'}{2},t'-\frac{\tau'}{2}\right)\mathcal{W}_2(t'',\omega''). \quad (11)$$

We next define a mixed time-frequency response function

$$\mathcal{S}^{(3)}(t'',\omega'',t',\omega') = \int_{-\infty}^{\infty} d\tau'\, S^{(3)}\left(t'',\omega'',t'+\frac{\tau'}{2},t'-\frac{\tau'}{2}\right)e^{i\tau'\omega'}$$

which relates to the temporal response function through a double Fourier transform

$$\mathcal{S}^{(3)}(t'',\omega'',t',\omega') = \iint_{-\infty}^{\infty} d\tau' d\tau''\, e^{i\omega'\tau'} e^{i\omega''\tau''} \cdot S^{(3)}\left(t''+\frac{\tau''}{2},t'+\frac{\tau'}{2},t'-\frac{\tau'}{2},t''-\frac{\tau''}{2}\right).$$

Equation (11) finally assumes the form

$$I_{\mathrm{PP}} = \frac{1}{(2\pi)^2}\iint_{-\infty}^{\infty} dt'\, dt'' \cdot \iint_{-\infty}^{\infty} d\omega'\, d\omega'' \mathcal{W}_2(t'',\omega'')\mathcal{S}^{(3)}(t'',\omega'',t',\omega')\mathcal{W}_1(t',\omega'). \quad (12)$$

This constitutes our final expression for the pump-probe signal whereby all quantities (the pump, the probe, and the material) are described by a mixed time-frequency representation.

The response function $S^{(3)}(t_1,t_2,t_3,t_4)$ can be calculated as a combination of the four-point correlation functions [26]

$$F^{(4)}(\tau_1,\tau_2,\tau_3,\tau_4) \equiv \langle V(\tau_1)V(\tau_2)V(\tau_3)V(\tau_4)\rangle. \quad (13)$$

Here, $V(t)$ is the dipole operator in the interaction picture, whose time evolution is given by the purely material Hamiltonian H_0, in the absence of external electric fields as

$$V(t) \equiv \exp\left\{\frac{i}{\hbar}\int_{-\infty}^{t} H_0(\tau)\, d\tau\right\}V(-\infty) \cdot \exp\left\{-\frac{i}{\hbar}\int_{-\infty}^{t} H_0(\tau)\, d\tau\right\}.$$

In the impulsive limit

$$\mathcal{W}_1(t',\omega') = \mathcal{W}_1\delta(t'-t_1)$$
$$\mathcal{W}_2(t'',\omega'') = \mathcal{W}_2\delta(t''-t_2)$$

where t_1 and t_2 are the times of the interactions with the pump and probe pulses, the signal (11) takes the form

$$I_{\mathrm{PP}}(t_2-t_1) = 4\mathcal{W}_1\mathcal{W}_2[F^{(4)}(t_1,t_2,t_2,t_1)+F^{(4)}(t_2,t_2,t_1,t_1)].$$

In the opposite case of ideal frequency-resolved detection, written as

$$\mathcal{W}_1(t',\omega') = \mathcal{W}_1\delta(\omega'-\omega_1)$$
$$\mathcal{W}_2(t'',\omega'') = \mathcal{W}_2\delta(\omega''-\omega_2)$$

we return to the original time variables (t,τ,τ',τ'') and obtain

$$I_{\mathrm{PP}}(\omega_2,\omega_1) = \overline{S}^{(3)}(-\omega_2,\omega_2,-\omega_1,\omega_1)$$

where $\overline{S}^{(3)}(-\omega_2,\omega_2,-\omega_1,\omega_1)$ is the frequency-domain susceptibility defined by

$$\overline{S}^{(3)}(\omega_1,\omega_2,\omega_3,\omega_4) = \iiiint_{-\infty}^{\infty} dt_1\, dt_2\, dt_3\, dt_4 S^{(3)}(t_1,t_2,t_3,t_4) \cdot \exp(i\omega_1t_1+i\omega_2t_2+i\omega_3t_3+i\omega_4t_4).$$

IV. Incoherent Autocorrelation Measurements: Gated Spontaneous Light Emission

In order to observe the autocorrelation signal, the field emitted by the sample ideally passes through two gating devices, a spectral gate whose transmission function is centered around ω_0 and a time gate centered at t_0. The measured signal (the total energy received by the detector) is given by (1), except that the field now passes through gating devices prior to its detection. Therefore, the signal becomes a function of both ω_0 and t_0, thus retaining its time and frequency information. The gated autocorrelation signal is defined as

$$I_{\mathrm{auto}}(t_0,\omega_0) \propto \int_{-\infty}^{\infty} \langle \mathcal{E}_j^*(t)\mathcal{E}_j(t)\rangle\, dt \quad (14)$$

where $\mathcal{E}$ is the gated field.

We show in the Appendix that the gated signal $I_{\mathrm{auto}}(t_0,\omega_0)$ can be recast in the form

$$I_{\mathrm{auto}}(t_0,\omega_0) = \iint_{-\infty}^{\infty} \frac{dt'\, d\omega'}{2\pi}\Phi(t',\omega';t_0,\omega_0)I'_{\mathrm{auto}}(t',\omega') \quad (15)$$

where

$$I'_{\mathrm{auto}}(t',\omega') = \int_{-\infty}^{\infty} \langle \mathcal{P}^*(t'-\tau/2)\mathcal{P}(t'+\tau/2)\rangle e^{i\omega'\tau}\, d\tau \quad (16)$$

is the bare autocorrelation signal corresponding to an ideal infinitely-resolved gating both in time and frequency, and $\Phi(t',\omega';t_0,\omega_0)$ is the joint gate function that depends on the transmission functions of the gates as well as the order in which they are applied. This function is precisely defined in the Appendix. The bare signal is not positive definite and it may even assume negative values. This is not the case for the gated signal, which is written as the squared amplitude (of the gated field) and is therefore always positive. The gate function $\Phi(t',\omega';t_0,\omega_0)$ is usually localized in both time and frequency. An ideal time gate, $\Phi(t',\omega';t_0,\omega_0) = \delta(t_0-t')$, yields the time-resolved signal,

$$I_{\mathrm{auto}}(t_0) = |P(t_0)|^2 \quad (17)$$

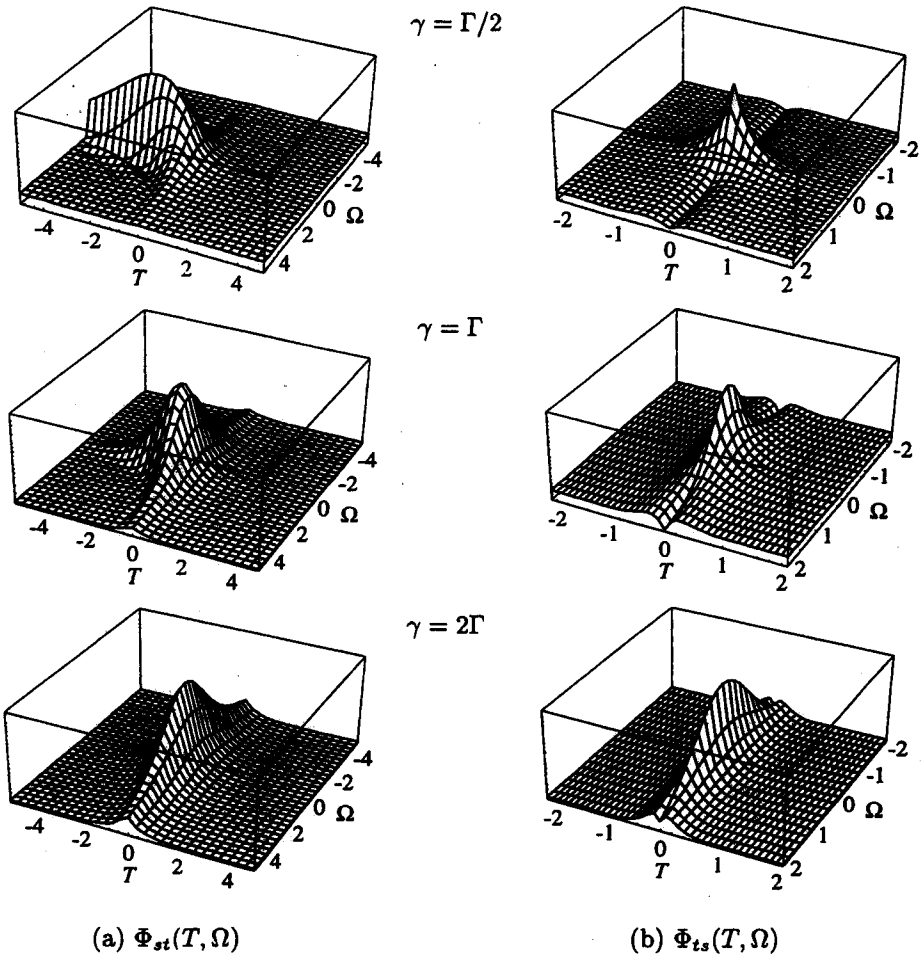

Fig. 1. The joint gate functions for the Fabry–Perot spectral gate and exponential time gate. (a) $\Phi_{st}(T,\Omega)$ representing spectral gate first (41). (b) $\Phi_{ts}(T,\Omega)$ representing time gate first (43). The frequency Ω is displayed in the units of Γ, the time T in the units of $1/\Gamma$. Note the different scales on the axes of the two columns.

whereas an ideal spectral gate, $\Phi(t',\omega';t_0,\omega_0)=\delta(\omega_0-\omega')$, gives the frequency-resolved signal

$$I_{\text{auto}}(\omega_0)=|P(\omega_0)|^2. \tag{18}$$

Note, however, that an ideal temporal and spectral gate, $\Phi(t',\omega';t_0,\omega_0)=\delta(t_0-t')\delta(\omega_0-\omega')$, cannot be realized due to the fundamental uncertainty of Fourier transform $\Delta\omega\Delta t\geq 1$.

In the Appendix, we give an example of the gate function, in which the spectral gate is given by the Fabry–Perot étalon, with the spectral width γ [12], and the time gate has an exponential transmission function with characteristic time Γ^{-1}. For this model, the gate function $\Phi(T,\Omega)$ only depends on $T\equiv t'-t_0$ and $\Omega\equiv\omega'-\omega_0$. In Fig. 1, we compare the resulting gate function assuming spectral gate first (left column), or time gate first (right column), for different ratios of γ/Γ. This ratio controls the selectivity of the gate: for $\gamma/\Gamma<1$ the gate has a narrow spectral transmission function and for $\gamma/\Gamma>1$ a narrow temporal function. We can also see that the order in which the gates are applied is important, especially for small γ/Γ.

Autocorrelation signals can be either coherent, representing the in-phase emission of many molecules, or incoherent, where we add the contributions of various molecules to the signal (rather than the amplitude). The former case will be treated in the next section where we make a specific application to three-pulse echoes. In this section, we consider an incoherent technique, spontaneous light emission, and the signal will be denoted as $I_{\text{SLE}}(t,\omega)$. We calculate $\langle\mathcal{P}^*(t-\tau/2)\mathcal{P}(t+\tau/2)\rangle$ to second order in the external field, and invoke the rotating-wave approximation. By expressing the polarization in terms of the response function convoluted with the external field, we get

$$\begin{aligned}\langle\mathcal{P}^*(t-\tau/2)\mathcal{P}(t+\tau/2)\rangle &= \int_0^\infty\!\!\int d\tau_1\, d\tau_2\, \mathcal{E}^*(t-\tau_1+\tau/2)\mathcal{E}(t-\tau_2-\tau/2)\\ &\quad\cdot F^{(4)}\Big(t-\tau_1+\frac{\tau}{2},t+\frac{\tau}{2},t-\frac{\tau}{2},t-\tau_2-\frac{\tau}{2}\Big)\end{aligned} \tag{19}$$

where $F^{(4)}(t_1,t_2,t_3,t_4)$ is the four-point correlation function of the dipole operator defined in (13). The Liouville-space path diagram corresponding to this correlation function is shown in Fig. 2.

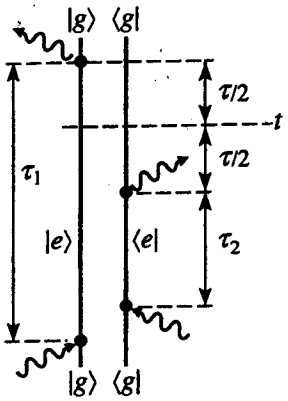

Fig. 2. The Liouville-space Feynman diagram representing the only term that contributes to the spontaneous light emission in the two-level system within RWA (19).

We now rewrite this expression using the Wigner distribution for the external field,

$$\mathcal{W}_{\mathcal{E}}(t,\omega)=\int_{-\infty}^{\infty}\mathcal{E}^{*}(t-\tau/2)\mathcal{E}(t+\tau/2)e^{i\omega\tau}\,d\tau. \tag{20}$$

Substituting (19) and (20) into (16), we obtain the bare signal

$$\begin{aligned}I'_{\mathrm{SLE}}(t',\omega)&=\frac{1}{2\pi}\int_{-\infty}^{\infty}d\tau\iint_{0}^{\infty}d\tau_1\,d\tau_2\int_{-\infty}^{\infty}d\omega_1\,e^{i\omega\tau}e^{-i\omega_1(\tau_1-\tau_2-\tau)}\\&\cdot F^{(4)}\left(t'-\tau_1+\frac{\tau}{2},t'+\frac{\tau}{2},t'-\frac{\tau}{2},t'-\tau_2-\frac{\tau}{2}\right)\\&\cdot\mathcal{W}_{\mathcal{E}}\left(t'-\frac{\tau_1+\tau_2}{2},\omega_1\right).\end{aligned} \tag{21}$$

We next change variables $\tau_2+\tau_1\rightarrow 2\tau',\tau_2-\tau_1+\tau\rightarrow\tau''$ and define the mixed time-frequency representation of the four-point correlation function

$$\begin{aligned}\mathcal{F}^{(4)}(t'',\omega'';t',\omega')&=\iint_{-\infty}^{\infty}d\tau'\,d\tau''\,e^{i\omega'\tau'}e^{i\omega''\tau''}\\&\cdot F^{(4)}\left(t''+\frac{\tau''}{2},t'+\frac{\tau'}{2},t'-\frac{\tau'}{2},t''-\frac{\tau''}{2}\right).\end{aligned} \tag{22}$$

Similar to the response functions in Section II, we define

$$F^{(4)}(t_1,t_2,t_3,t_4)\equiv 0\quad\text{for } t_1>t_2,t_4>t_3$$

thus extending the integrals in (22) to infinity. The gated signal (15) finally takes the form

$$I_{\mathrm{SLE}}(t_0,\omega_0)=\iint_{-\infty}^{\infty}\frac{dt'\,d\omega'}{2\pi}\Phi(t',\omega';t_0,\omega_0)I'_{\mathrm{SLE}}(t',\omega') \tag{23}$$

where the bare signal (21) is given by

$$I'_{\mathrm{SLE}}(t',\omega)=\iint_{-\infty}^{\infty}\frac{d\tau'\,d\omega_1}{2\pi}\mathcal{F}^{(4)}(t'-\tau',\omega_1;t',\omega)\mathcal{W}_{\mathcal{E}}(t'-\tau',\omega_1).$$

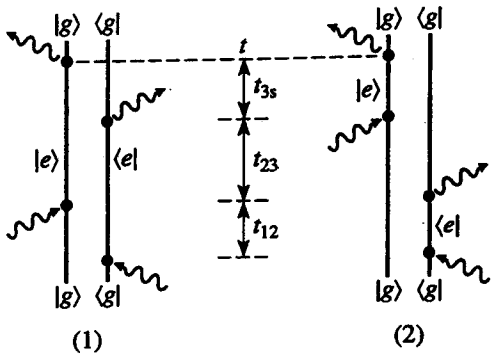

Fig. 3. Liouville-space Feynman diagrams for $R_j^{(3)}(t_{3s},t_{23},t_{12}),j=1,2$.

In this expression, the signal is given by a convolution of a material response function, a Wigner function for the pump field, and a detection gate function, all written in a mixed time-frequency representation.

V. Coherent Autocorrelation Measurements: Gated Three-Pulse Echoes

In this section, we will focus on coherent autocorrelation signals, obtained when the fields $\mathcal{E}_s^{*}(t-\tau/2)$ and $\mathcal{E}_s(t+\tau/2)$ are generated by contributions of many uncorrelated molecules, so that the quantum mechanical autocorrelation function in the integrand of (16) can be factorized as $\langle\mathcal{P}_s^{*}(t'-\tau/2)\rangle\langle\mathcal{P}_s(t'+\tau/2)\rangle$. We thus have

$$\begin{aligned}I'_{\mathrm{coh}}(t',\omega';\boldsymbol{k}_s)&=\int_{-\infty}^{\infty}\langle\mathcal{P}_s^{*}(t'-\tau/2)\rangle\langle\mathcal{P}_s(t'+\tau/2)\rangle e^{i\omega'\tau}\,d\tau.\end{aligned} \tag{24}$$

As an illustration, we calculate the gated three-pulse echo for a two-level chromophore. Consider the coherent signal (24) in a four-wave mixing experiment involving three laser pulses:

$$\begin{aligned}E(\boldsymbol{r},t)&=\mathcal{E}_1(t+t_{12}+t_{23})e^{i\boldsymbol{k}_1\boldsymbol{r}}\\&+\mathcal{E}_2(t+t_{12})e^{i\boldsymbol{k}_2\boldsymbol{r}}+\mathcal{E}_3(t)e^{i\boldsymbol{k}_3\boldsymbol{r}}+\text{c.c.}\end{aligned}$$

We assume that pulse 1 comes first, then 2, and finally 3; t_{12} and t_{23} are the (positive) time delays between the pulses. We calculate the signal with the outgoing wavevector $\boldsymbol{k}_s=\boldsymbol{k}_3+\boldsymbol{k}_2-\boldsymbol{k}_1$, and frequency $\omega_s=\omega_3+\omega_2-\omega_1$, measured at times t_{3s} after pulse 3. The polarization $\mathcal{P}(t_{3s})$ to third order in the external field is given in [7]. Assuming that the pulses are short compared with all relevant material timescales (impulsive measurements), and selecting the terms that contribute to the photon echo signal, we have

$$\langle\mathcal{P}_{\mathrm{PE}}^{(3)}(\boldsymbol{k}_{s,t_{3s}})\rangle=\mathcal{R}^{(3)}(t_{3s},t_{23},t_{12})$$

where

$$\begin{aligned}&\mathcal{R}^{(3)}(t_{3s},t_{23},t_{12};\boldsymbol{k}_s)\\&\quad\equiv R_1^{(3)}(t_{3s},t_{23},t_{12})+R_2^{(3)}(t_{3s},t_{23},t_{12})\\&R_1^{(3)}(t_{3s},t_{23},t_{12})\\&\quad=F^{(4)}(t-t_{3s}-t_{23},t,t-t_{3s},t-t_{3s}-t_{23}-t_{12})\\&R_2^{(3)}(t_{3s},t_{23},t_{12})\\&\quad=F^{(4)}(t-t_{3s},t,t-t_{3s}-t_{23},t-t_{3s}-t_{23}-t_{12})\end{aligned} \tag{25}$$

and $F^{(4)}$ is the four-point correlation function as defined in (13). The Liouville-space paths corresponding to $R_j^{(3)}$ are shown in Fig. 3, and the signal can then be written as

$$I'_{\mathrm{coh,PE}}(t_{3s},\omega') = \int_{-\infty}^{\infty} \mathcal{R}^{(3)^*}\left(t_{3s}-\frac{\tau}{2},t_{12},t_{23}\right)\mathcal{R}^{(3)} \cdot\left(t_{3s}+\frac{\tau}{2},t_{12},t_{23}\right)e^{i\omega'\tau}\,d\tau. \quad (26)$$

We will apply this result to a two electronic-level model with several primary nuclear harmonic modes coupled linearly to the electronic system. The nuclear degrees of freedom are in turn coupled to a harmonic oscillator bath. This Brownian oscillator model provides a realistic description of condensed phase systems by incorporating homogeneous and inhomogeneous dephasing, spectral diffusion, and quantum beats in a unified fashion. The response functions (26) take the form [7]

$$\begin{aligned} R_1(t_{3s},t_{12},t_{23}) &= \exp\{i\omega_{eg}(t_{3s}-t_{23})\} \\ &\cdot\exp\{-g^*(t_{3s})-g^*(t_{23})+g(t_{12})-g(t_{12}+t_{3s}) \\ &-g^*(t_{12}+t_{23})+g^*(t_{12}+t_{23}+t_{3s})\} \\ R_2(t_{3s},t_{12},t_{23}) &= \exp\{i\omega_{eg}(t_{3s}-t_{23})\} \\ &\cdot\exp\{-g(t_{3s})-g^*(t_{23})+g^*(t_{12})-g^*(t_{12}+t_{3s}) \\ &-g^*(t_{12}+t_{23})+g^*(t_{12}+t_{23}+t_{3s})\} \end{aligned}$$

where ω_{eg} is the electronic transition frequency and the function $g(t)$ is given by

$$g(t)=\sum_j^N g_j(t)$$

where N is the number of Brownian oscillator modes, and $g_j(t)$ is related to the nuclear spectral density $\tilde{C}_j(\omega)$ that carries all the necessary microscopic information [7]

$$g_j(t) = -\frac{1}{2\pi}\int_{-\infty}^{\infty}\frac{d\omega}{\omega^2}\tilde{C}_j(\omega)[\exp(-i\omega t)+i\omega t-1].$$

Here, we consider the limiting case of overdamped modes in the high-temperature limit $\beta\hbar\Lambda \ll 1$, which are typical for low-frequency solvent modes. In this case, $\gamma_j \gg 2\omega_j$, where γ_j is the coupling strength of a primary oscillator to the bath. We have

$$\begin{aligned} g_j(t) &= \left[\frac{2\lambda_j}{\beta\hbar\Lambda_j^2}-i\left(\frac{\lambda_j}{\Lambda_j}\right)\right][e^{-\Lambda_j t}+\Lambda_j t-1] \\ \lambda_j &\equiv \frac{\hbar}{2m_j\omega_j^2}, \quad \Lambda_j \equiv \frac{\omega_j^2}{\gamma_j}. \end{aligned} \quad (27)$$

In the inhomogeneous limit $\kappa^2 \equiv \beta\hbar\Lambda_j^2/2\lambda_j \ll 1$, the nuclear dynamics (with timescale Λ_j^{-1}) are slow, and this formula reduces to

$$g_j(t)=\eta^2 t^2, \quad \eta^2 \equiv \sum_{j=1}^N \frac{\lambda_j}{\beta\hbar}.$$

The response function (26) then takes the form

$$\mathcal{R}^{(3)}(t_{3s},t_{12},t_{23}) = 2e^{i\omega_{eg}(t_{3s}-t_{23})}e^{-\eta^2(t_{3s}-t_{23})^2}$$

and the bare signal (26) assumes the Gaussian shape in both time and frequency as

$$\begin{aligned} &I'_{\mathrm{coh,PE}}(t_{3s},\omega') \\ &\quad = \exp\{-2\eta^2(t_{3s}-t_{23})^2\}\exp\left\{-\frac{(\omega'-\omega_{eg})^2}{2\eta^2}\right\}. \end{aligned} \quad (28)$$

In the other extreme, $\kappa \gg 1$, the nuclear dynamics are fast compared with the coupling strength, and (27) reduces to

$$g(t)=\hat{\Gamma}t-i\lambda t, \quad \hat{\Gamma}\equiv\sum_{j=1}^N\frac{2\lambda_j}{\beta\hbar\Lambda_j}, \quad \lambda\equiv\sum_{j=1}^N\lambda_j.$$

We then have

$$\mathcal{R}^{(3)}(t_{3s},t_{12},t_{23}) = 2e^{i\omega_{eg}(t_{3s}-t_{23})}e^{-\hat{\Gamma}(t_{3s}+t_{23})}e^{-i\lambda(t_{3s}-t_{23})}$$

which yields for the bare signal

$$I'_{\mathrm{coh,PE}}(t_{3s},\omega') = \exp\{-2\hat{\Gamma}(t_{3s}+t_{23})\}\delta(\omega'-\omega_{eg}+\lambda). \quad (29)$$

In Fig. 4, we display the bare signals for various values of κ. The first column shows the signal $I'_{\mathrm{coh,PE}}(t,\omega)$, and the second and the third columns represent this signal integrated over frequency and time, respectively. For comparison, we also present the linear absorption lineshape (dashed line) in the third column [7],

$$\sigma(\omega') = \mathrm{Re}\int_{-\infty}^{\infty} e^{i(\omega'-\omega_{eg})t-g(t)}\,dt. \quad (30)$$

For small κ [Fig. 4(a)], we see the echo signal at $t_{3s}=t_{23}$ as given by (28). As κ increases, the echo shifts toward smaller values of t_{3s} and finally vanishes completely. In addition, the signal becomes spectrally narrower, and for large κ [Fig. 4(e)] (times that are not too short) tends to the limit given by (29). We also see how the frequency shifts as we go from the inhomogeneous to the homogeneous limit: for small κ, the spectrum is centered at $\omega=\omega_{eg}$, whereas for large κ at $\omega=\omega_{eg}+\lambda$. All the signals in Fig. 4 are normalized to 1 at the maximum.

To illustrate the effect of the gate, we consider the bare signal in the inhomogeneous limit and assume that the spectral and time gates are given by (39) and (40). The signal is then calculated by (15) as a convolution of the bare signal (28) and the joint gate function calculated in the Appendix [see (42)] as

$$\begin{aligned} I_{\mathrm{coh,PE}}(t_0,\omega_0) = \iint_{-\infty}^{\infty}&\frac{dt_{3s}\,d\omega'}{2\pi}\,\frac{e^{-2\Gamma|t_{3s}-t_0|}}{(\omega'-\omega_0)^2+\Gamma^2} \\ &\cdot\exp\{-2\eta^2(t_{3s}-t_{23})^2\} \\ &\cdot\exp\left\{-\frac{(\omega'-\omega_{eg})^2}{2\eta^2}\right\}. \end{aligned}$$

Fig. 5 shows how the nature of the signal varies, depending on the relative magnitude of the parameters η and Γ. If $\Gamma \gg \eta$, the gate provides high temporal resolution, and the gated signal has the same temporal shape as the bare one. On the other hand, if $\Gamma \ll \eta$, we can improve spectral resolution by sacrificing the time resolution. We present in

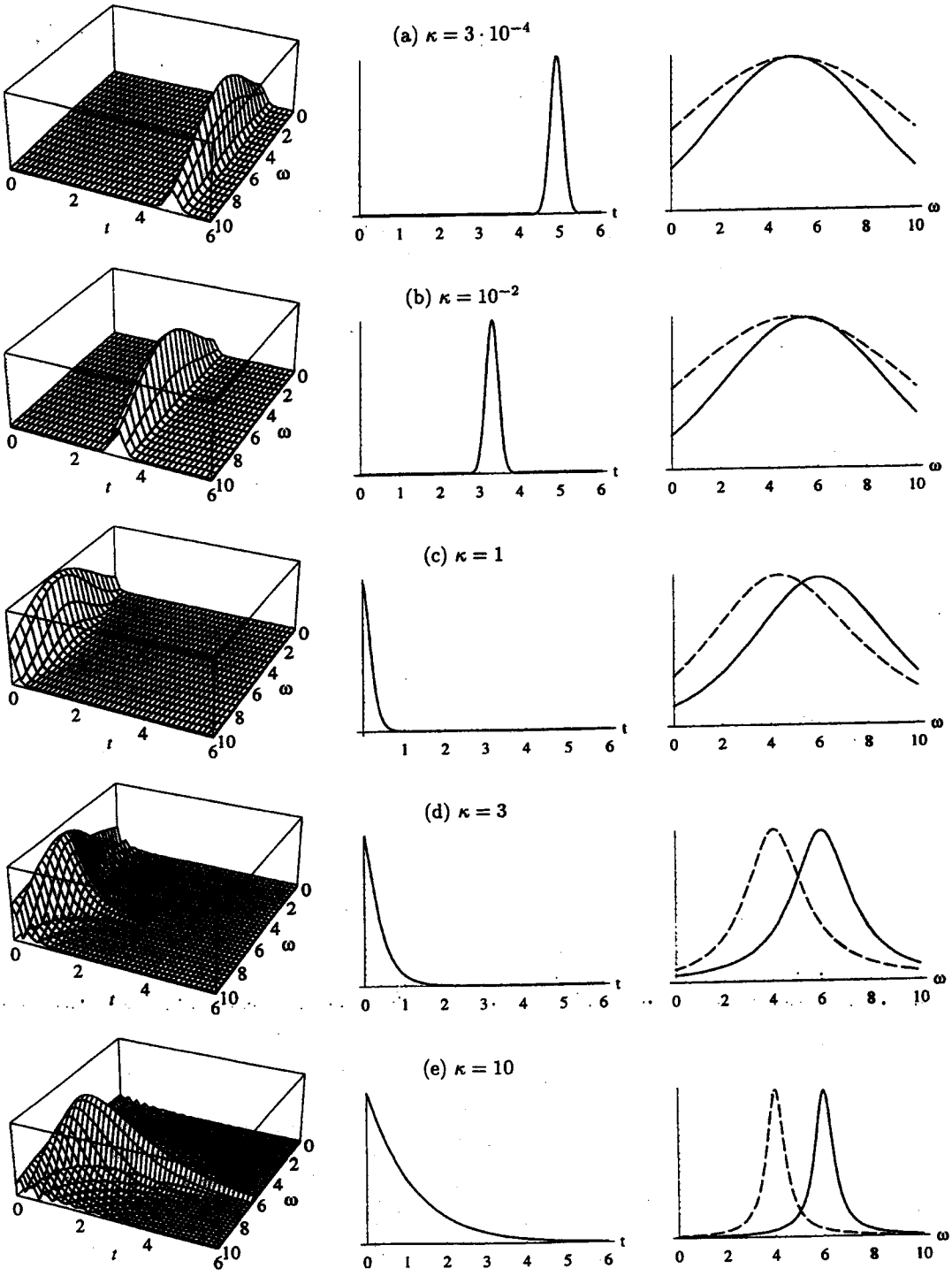

Fig. 4. Three-pulse echo signal (26) for one overdamped Brownian oscillator calculated for different values of the parameter κ. The first column represents the signal $I_{\mathrm{coh,PE}}(t,\omega)$, and the second and the third give the same signal integrated over frequency and time, respectively. The dashed line in the third column is the absorption spectrum (30). Time (frequency) are expressed in the units of $\lambda^{-1}(\lambda)$. The transition frequency is $\omega_{eg} = 5\lambda$. The temperature is $\beta\hbar\lambda = 0.1$ and the time intervals $t_{12} = t_{23} = 5\lambda^{-1}$.

Fig. 5 the bare signal (28) [Fig. 5(a)] and the gated signals for $\Gamma = \eta/5, \Gamma = \eta/2.2$, and $\Gamma = \eta$ [Fig. 5(b)–(d)]. In all the plots, we used $\gamma = 5\Gamma$.

VI. Conclusion

The formal results as well as the calculations presented here clearly demonstrate the usefulness of mixed time-frequency representations of optical signals. Such representations provide a clear physical insight most valuable for the interpretation and the computation of optical measurements. With this picture, both the light pulses and the gates enter in the signal as double frequency and time convolutions with a "bare" purely material signal. Thus, the role of the probe pulse in pump-probe

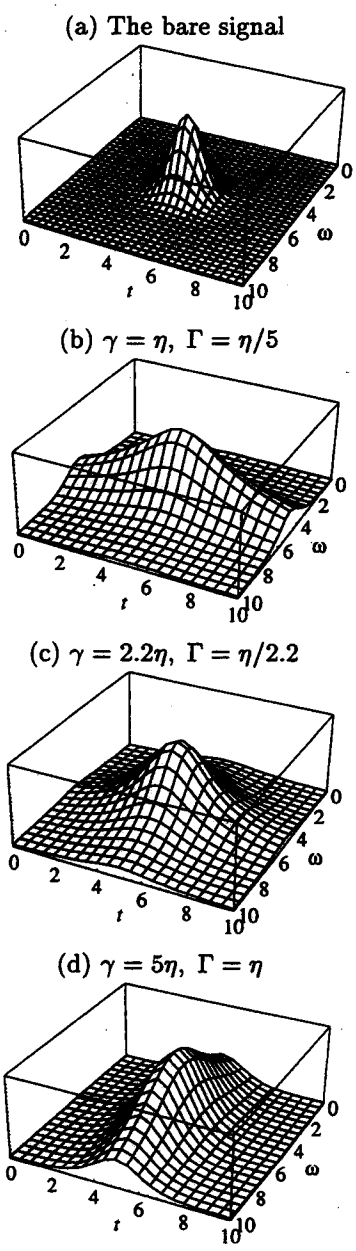

Fig. 5. Gated three-pulse echo. Model and parameters are the same as in Fig. 4(a) except that $\beta\hbar\lambda = 2$. We use the gate function (42) representing the Fabry–Perot étalon and the time gate with the exponential time profile. The bare signal (a) and the gated signals for different temporal widths of the gate transmission function relative to the width of the bare signal (b)–(d) are shown. For $\Gamma \ll \eta$ ($\Gamma \gg \eta$) we obtain the enhancement of spectral (temporal) resolution.

spectroscopy is shown to be very similar to that of the optical gate in fluorescence measurements. The time- and frequency-resolved signal provides information about the time-dependent phase of the signal field. In fluorescence measurements, for example, (15) shows the time-dependent Stokes shift, which reflects solvent dynamics [5]. This information is not contained in the integrated signals (17) and (18). The same conclusions hold also for other nonlinear measurements. The gated signal of some low-order processes formally contains information that requires higher order nonlinearities with integrated detection, since it depends on a correlation function that contains additional time variables. Detailed studies, which could clarify the relevant information (e.g., homogeneous versus inhomogeneous broadening) and show the best detection mode, can be made using, for example, the multimode Brownian oscillator model.

Appendix
Time- and Frequency-Gated Autocorrelation Signal

We consider a setup in which the emitted field passes through two gating devices, a spectral and a time gate. The spectral gate is a spectrometer, which transmits energy in a specific frequency interval centered near some selected frequency ω_0. We will characterize it by the spectral transmission function $\mathcal{F}_s(\omega;\omega_0)$, and the gated field is

$$\mathcal{E}(\omega) = \mathcal{F}_s(\omega;\omega_0)\mathcal{E}'(\omega). \tag{A1}$$

Here $\mathcal{E}'(\omega)$ and $\mathcal{E}(\omega)$ are the fields before and after passing through the gate, respectively. We shall denote them the bare and the gated signal, and throughout this section, bare quantities will be denoted by a prime ($'$).

Equation (A1) can be rewritten in time domain using the convolution

$$\mathcal{E}(t) = \int_{-\infty}^{\infty} \mathcal{F}_s(t-t_1;\omega_0)\mathcal{E}'(t_1)\,dt_1. \tag{A2}$$

For reasons of causality, $\mathcal{F}_s(\tau;\omega_0)$ must vanish identically for $\tau < 0$.

The time gate acts in the time domain similar to the spectral gate in frequency domain: it transfers the field for a short time interval centered around t_0. The gated field is

$$\mathcal{E}(t) = \mathcal{F}_t(t;t_0)\mathcal{E}'(t) \tag{A3}$$

where $\mathcal{F}_t(t;t_0)$ is the temporal transmission function. Note that the order in which the two gates are applied is important, even though both devices are linear and independently adjustable. However, signals obtained for different orders of the gates carry equivalent information regarding the bare field [27]. From a practical point of view, to attain optimal time and frequency resolution, it is advantageous to apply first the gate with the less-ideal transfer function [27]. Below we will consider both configurations.

We start with the case when the spectral gate is applied first. The field after passing both gates is obtained by combining (A2) and (A3):

$$\mathcal{E}(t) = \int_{-\infty}^{\infty} \mathcal{F}_t(t;t_0)\mathcal{F}_s(t-t_1;\omega_0)\mathcal{E}'(t_1)\,dt_1.$$

The measured signal (the total energy received by the detector) is given by (14). In terms of the polarization, it can be written as

$$I_{\text{auto}} = \iiint_{-\infty}^{\infty} dt\,dt_1\,dt_2 |\mathcal{F}_t(t;t_0)|^2 \cdot \mathcal{F}_s^*(t-t_1;\omega_0)\mathcal{F}_s(t-t_2;\omega_0) \cdot \langle \mathcal{P}^*(t_1)\mathcal{P}(t_2)\rangle. \tag{A4}$$

We now introduce the Wigner function for the spectral gate

$$\mathcal{W}_s(t,\omega'') = \int_{-\infty}^{\infty} \mathcal{F}_s^*(t-\tau/2)\mathcal{F}_s(t+\tau/2)e^{i\omega''\tau}\,d\tau$$

and define the bare autocorrelation signal (16).

Substituting this into (A4), we obtain

$$I_{\text{auto}} = \iiint_{-\infty}^{\infty} dt\,dt_1\,dt_2 \int\int_{-\infty}^{\infty} \cdot \frac{d\omega'\,d\omega''}{(2\pi)^2} e^{i(t_2-t_1)(\omega''-\omega')}|\mathcal{F}_t(t;t_0)|^2 \cdot \mathcal{W}_s\left(t-\frac{t_1+t_2}{2},\omega''\right) I'_{\text{auto}}\left(\frac{t_1+t_2}{2},\omega'\right).$$

We further change the variables $t_1+t_2 \to 2t', t_2-t_1 \to t''$, calculate the integrals with respect to t'' and ω'', and the autocorrelation signal assumes the final form

$$I_{\text{auto}}(t_0,\omega_0) = \iint_{-\infty}^{\infty} \frac{dt'\,d\omega'}{2\pi}\Phi(t',\omega';t_0,\omega_0)I'_{\text{auto}}(t',\omega') \tag{A5}$$

where we defined the joint gate function that includes the characteristics of both the spectral and time gates

$$\Phi_{st}(t',\omega';t_0,\omega_0) = \int_{-\infty}^{\infty} dt|\mathcal{F}_t(t;t_0)|^2\mathcal{W}_s(t-t',\omega';\omega_0). \tag{A6}$$

The subscript st indicates that the signal first passes through the spectral gate and then though the time gate.

Assuming specific forms of the time and spectral gates, we get the signal measured in different experimental setups. If the time gate is infinitely short, $\mathcal{F}_t(t;t_0) = \delta(t-t_0)$, we obtain the spectrograms discussed in [12]. If the signal passes only through the time gate, then the gate acts like the reference pulse in the FROG configuration.

It is convenient to define also the Wigner function for the time gate

$$\mathcal{W}_t(t,\omega) = \int_{-\infty}^{\infty} \mathcal{F}_t^*(t-\tau/2)\mathcal{F}_t(t+\tau/2)e^{i\omega\tau}\,d\tau.$$

The joint gate function (A6) then assumes the form

$$\Phi_{st}(t',\omega';t_0,\omega_0) = \iint_{-\infty}^{\infty} \frac{dt\,d\omega}{2\pi}\mathcal{W}_t(t,\omega;t_0)\mathcal{W}_s(t-t',\omega';\omega_0). \tag{A7}$$

This gate function is centered around the frequency ω_0 and the time t_0 and acts as a filter on the bare signal I'. The gated signal can be calculated as a convolution of the gate function $\Phi_{st}(t',\omega';t_0,\omega_0)$ and the bare signal (15).

When the time gate is applied first, we can write the signal in the same form. The gated field is then written as

$$\mathcal{E}(t) = \int_{-\infty}^{\infty} \mathcal{F}_s(t-t_1;\omega_0)\mathcal{F}_t(t';t_0)\mathcal{E}'(t_1)$$

and if we define the joint gate function as

$$\Phi_{ts}(t',\omega';t_0,\omega_0) = \iint_{-\infty}^{\infty} \frac{dt\,d\omega}{2\pi}\mathcal{W}_s(t,\omega;\omega_0)\mathcal{W}_t(t',\omega-\omega';t_0) \tag{A8}$$

or, after calculating the integral with respect to t,

$$\Phi_{ts}(t',\omega';t_0,\omega_0) = \int_{-\infty}^{\infty} \frac{d\omega}{2\pi}|\mathcal{F}_s(\omega;\omega_0)|^2\mathcal{W}_t(t',\omega-\omega';t_0)$$

we recast (15) for the gated autocorrelation signal with the joint gate function (A8) instead of (A7).

As an example, we shall consider the case when the spectral gate is given by the Fabry–Perot étalon [12], and the time gate is exponential,

$$\mathcal{F}_s(\omega;\omega_0) = \frac{\gamma}{\gamma - i(\omega-\omega_0)} \tag{A9}$$

$$\mathcal{F}_t(t;t_0) = e^{-\Gamma|t-t_0|}. \tag{A10}$$

Note that the transmission functions (A9) and (A10) depend on t, t_0 and ω, ω_0 only through the combinations $t-t_0$ and $\omega-\omega_0$. In this case, the joint gate function $\Phi_{st}(t',\omega';t_0,\omega_0)$ only depends on $T \equiv t'-t_0$ and $\Omega \equiv \omega'-\omega_0$. The joint gate function for the gates (A9) and (A10), calculated by (A6), assumes the form

$$\Phi_{st}(T,\Omega) = \begin{cases} \dfrac{e^{-2\Gamma T}}{\Omega^2+(\Gamma+\gamma)^2}, & T>0 \\ \dfrac{e^{2\Gamma T}}{\Omega^2+(\Gamma-\gamma)^2} - \dfrac{4\Gamma e^{2\gamma T}}{(\Omega^2+\Gamma^2+\gamma^2)^2-4\Gamma^2\gamma^2} \times\left\{\gamma\cos 2\Omega T - \dfrac{\Omega^2+\Gamma^2-\gamma^2}{2\Omega}\sin 2\Omega T\right\}, & T<0. \end{cases} \tag{A11}$$

In the case $\gamma \gg \Gamma$, the above expression simplifies and can be written in the compact form

$$\Phi_{st}(T,\Omega) = \frac{e^{-2\Gamma|T|}}{\Omega^2+\gamma^2}. \tag{A12}$$

For the reverse order of gates (time gate first), we have

$$\Phi_{ts}(T,\Omega) = \frac{\Gamma}{\gamma}\frac{e^{-2(\gamma+\Gamma)|T|}}{[\Omega^2+(\gamma+\Gamma)^2](\Omega^2+\gamma^2)} \cdot\{[\Omega^2-\gamma(\gamma+\Gamma)]\cos 2\Omega T - (2\gamma+\Gamma)\sin 2\Omega|T|\}. \tag{A13}$$

The functions $\Phi_{st}(T,\Omega)$ and $\Phi_{ts}(T,\Omega)$ for different values of the parameters γ and Γ are shown in Fig. 1. More elaborate gating profiles may be obtained using pulse-shaping techniques.

REFERENCES

[1] W. S. Warren, H. Rabitz, and M. Dahleh, "Coherent control of quantum dynamics: The dream is alive," *Science*, vol. 259, p. 1581, 1993.

[2] B. Kohler, J. L. Krause, F. Raksi, C. Rose-Petruck, R. M. Whitnell, K. R. Wilson, V. V. Yakovlev, Y. Yan, and S. Mukamel, "Mode-locking matter with light," *J. Phys. Chem.*, vol. 97, p. 12602, 1993.

[3] A. M. Weiner, "Femtosecond optical pulse shaping and processing," *Prog. Quantum Electron.*, vol. 19, p. 161, 1995.

[4] J. T. Fourkas, L. Dhar, K. A. Nelson, and R. Trebino, "Spatially encoded, single-shot ultrafast spectroscopies," *J. Opt. Soc. Amer. B*, vol. 12, pp. 155–165, 1995.

[5] N. F. Scherer, L. D. Zeigler, and G. R. Fleming, "Heterodyne-detected time-domain measurement of I_2 predissociation and vibrational dynamics in solution," *J. Chem. Phys.*, vol. 96, p. 5544, 1992.

[6] B. Kohler, V. V. Yakovlev, J. Che, J. L. Krause, M. Messina, and K. R. Wilson, "Quantum control of wave packet evolution with tailored Femtosecond pulses," *Phys. Rev. Lett.*, vol. 74, pp. 3360–3363.

[7] S. Mukamel, *Principles of Nonlinear Optical Spectroscopy*. London, U.K.: Oxford Univ. Press, 1995.

[8] H. M. Nussenzweig, *Introduction to Quantum Optics*. New York: Gordon and Breach, 1973.

[9] E. T. J. Nibbering, D. A. Wiersma, and K. Duppen, "Femtosecond non-Markovian optical dynamics in solutions," *Phys. Rev. Lett.*, vol. 66, pp. 2464–2467, 1991.

[10] D. C. Arnett, P. Vöhringer, R. A. Westervelt, M. J. Feldstein, and N. F. Scherer, *Ultrafast Phenomena IX*, P. F. Barbara, W. H. Knox, G. A. Mourou, and A. H. Zewail, Eds. Berlin: Springer-Verlag, 1994.

[11] P. Vöhringer, D. C. Arnett, T.-S. Yang, and N. F. Scherer, "Time-gated photon-echo spectroscopy in liquids," *Chem. Phys. Lett.*, vol. 237, p. 387, 1995.

[12] H. Stolz, *Time-Resolved Light Scattering from Excitons*, Berlin: Springer, 1994.

[13] D. S. Chemla, J.-Y. Bigot, M.-A. Mycek, S. Weiss, and W. Schäfer, "Ultrafast phase dynamics of coherent emission from excitons in GaAs quantum wells," *Phys. Rev. A*, vol. 50, p. 8449, 1994.

[14] W. Koenig, H. K. Dunn, and L. Y. Lacy, "The sound spectrograph," *J. Acoust. Soc. Amer.*, vol. 18, p. 19, 1946.

[15] J. Paye, "The chronocyclic representation of ultrashort light pulses," *IEEE J. Quantum Electron.*, vol. 28, p. 2262, 1992.

[16] ———, "Applications of the chronocyclic representation of ultrashort light pulses," in *Ultrafast phenomena IX*, P. F. Barbara, W. H. Knox, G. A. Mourou, and A. H. Zewail, Eds. Berlin: Springer-Verlag, 1994, pp. 9–13.

[17] L. Cohen, "Time-frequency distributions—A review," *Proc. IEEE*, vol. 77, pp. 941–981, 1989.

[18] L. Mandel and E. Wolf, Eds., *Selected Papers on Coherence and Fluctuations of Light, with Bibliography*. New York: Dover, 1970.

[19] M. G. Raymer, M. Beck, and D. T. Smithey, "Measurement of the Wigner distribution and the density matrix of a light mode using optical homodyne tomography: Application to squeezed states and the vacuum," *Phys. Rev. Lett.*, vol. 70, pp. 1244–1247, 1993.

[20] K. H. Brenner and K. Wodkiewicz, "The time-dependent physical spectrum of light and the Wigner distribution function," *Opt. Commun.*, vol. 43, pp. 103–106, 1982.

[21] R. Gase, "Time-dependent spectrum of linear optical systems," *J. Opt. Soc. Amer. A*, vol. 8, p. 850, 1991.

[22] A. W. Rihaczek, *Principles of High-Resolution Radar*. New York: McGraw-Hill, 1969.

[23] R. A. Altes, "Detection, estimation, and classification with spectrograms," *J. Acoust. Soc. Amer.*, vol. 67, pp. 1232–1246, 1980.

[24] D. J. Kane and R. Trebino, "Characterization of arbitrary femtosecond pulses using frequency-resolved optical gating," *IEEE J. Quantum Electron.*, vol. 29, p. 571, 1993.

[25] R. Trebino and D. J. Kane, "Using phase retrieval to measure the intensity and phase of ultrashort pulses: Frequency-resolved optical gating," *J. Opt. Soc. Amer. A*, vol. 10, p. 1101, 1993.

[26] S. Mukamel, C. Ciordas-Ciurdariu, and V. Khidekel, "Wigner representation and nuclear wavepackets in nonlinear and spontaneous light emission spectroscopy," *Advances in Chem. Phys.*, submitted for publication.

[27] V. Wong and I. A. Walmsley, "A linear filter analysis of methods for ultrashort-pulse-shape measurements," *J. Opt. Soc. Amer. B*, vol. 12, p. 1491, 1995.

Shaul Mukamel received the Ph.D. degree in chemical physics in 1976 from Tel-Aviv University, Israel.

He conducted postdoctoral work at Massachusetts Institute of Technology, Cambridge, and the University of California, Berkeley. He is currently a Professor of chemistry at the University of Rochester, NY. His research interests include theoretical studies of ultrafast nonlinear optical spectroscopy in condensed phases, molecular and semiconductor nanostructures, optical materials, and biological electron and energy transfer. He is the author of over 300 publications and a graduate-level textbook, *Principles of Nonlinear Optical Spectroscopy*, (Oxford: Oxford Univ. Press, 1995).

Dr. Mukamel is a fellow of the American Physical Society and the American Chemical Society and a recipient of the Fulbright, Alfred P. Sloan, Camille and Henry Drefus, and Guggenheim fellowships.

Calin Ciordas-Ciurdariu was born in Bucharest, Romania, in 1968. He received M.S. degrees in physics from the University of Bucharest and the University of Rochester, NY, in 1993 and 1995, respectively.

Between 1992 and 1993, he worked as a Junior Scientist at the Institute for Physical Chemistry of the Romanian Academy of Science. Since 1993, he has been working toward the Ph.D. degree in physics at the University of Rochester.

Vadim Khidekel was born in Leningrad, USSR, in 1964. He received the M.S. degree from Leningrad State University in 1987 and the Ph.D. degree in chemical physics from School of Chemistry of Tel-Aviv University, Israel.

Since then, he has been working as a Postdoctoral Fellow in the Department of Chemistry, University of Rochester, NY. The main area of his research is nonlinear spectroscopy and ultrafast processes in optics and spectroscopy.